Open access • Journal Article • DOI:10.1108/EB023823

Robust finite elements for 3d-analysis of rubber-like materials — Source link

P.A.J. Van den Bogert, R. de Borst, G.T. Luiten, J. Zeilmaker

Institutions: Delft University of Technology

Published on: 01 Jan 1991 - Engineering Computations (MCB UP Ltd)

Topics: Finite element method and Constraint counting

ENGINEERING COMPUTATIONS VOL. 8, 3–17 (1991)

CONTRIBUTED Papers

ROBUST FINITE ELEMENTS FOR 3D-ANALYSIS OF RUBBER-LIKE MATERIALS

P. A. J. VAN DEN BOGERT

Department of Civil Engineering, Delft University of Technology, PO Box 5048, 2600 GA Delft, The Netherlands

R. DE BORST

TNO Institute for Building Materials and Structures/Department of Civil Engineering, Delft University of Technology, PO Box 5048, 2600 GA Delft, The Netherlands

G. T. LUITEN

Department of Civil Engineering, Delft University of Technology, PO Box 5048, 2600 GA Delft, The Netherlands

AND

J. ZEILMAKER

Rijkswaterstaat [formerly: TNO Centre for Polymeric Materials]

ABSTRACT

A marked characteristic of rubber-like materials is the nearly incompressible behaviour. This type of behaviour is best modelled by mixed finite elements with separate interpolation functions for the displacements and the pressure. In this contribution the performance of three-dimensional elements is investigated using a two-tiered strategy. First, the ability of some linear and quadratic three-dimensional elements to deform correctly under nearly isochoric conditions is estimated using the well-known constraint-counting method, in which the ratio of the number of degrees-of-freedom over the number of kinematic constraints present in the finite element mesh is determined. Next, the performance of the elements is assessed by numerical simulations for three cuboidal rubber blocks with different shape factors. The results turn out to be quite sensitive with respect to the ratio of the number of degrees-of-freedom over the number of kinematic constraints, since too many pressure degrees-of-freedom make the element overstiff, while too few pressure degrees-of-freedom may cause the occurrence of spurious kinematic modes. This observation appears to be not only valid for the global structural behaviour, but also with respect to the specific parts in the structure, where the above-mentioned ratio is different from the global number, e.g., in corners of the structure.

KEY WORDS Rubber-like materials Constraint counting Robust finite elements Three-dimensional analysis

INTRODUCTION

Rubbers are frequently used in engineering practice, e.g., for tyres, shock absorbers, seals and laminated bearing packages. Many of these structures are truly three-dimensional and

0264–4401/91/010003–15$2.00

Received July 1990

plane–stress or plane–strain idealizations cannot sufficiently accurately capture the mechanical behaviour. Accordingly, three-dimensional analyses are called for.

Here, the difficulty comes in. Not only are three-dimensional finite element analyses still relatively expensive, but rubber and rubber-like materials have the nasty property that they are almost incompressible. Typically, the ratio of the bulk modulus κ over the shear modulus μ in the ground state (the undeformed state) is around 1000. For conventional, displacement-based finite elements this inevitably implies that the amount of energy stored in volumetric deformations is severely overestimated, which gives an overstiff behaviour. This phenomenon is commonly known as locking. A possible remedy is to use separate interpolations for the displacements and the pressures, e.g., Sussman and Bathe[17]. Such a formulation results in a 'softer' element behaviour, giving a major improvement with respect to the computed displacements. When the pressure degrees-of-freedom are condensed out statically at an element level, only displacement degrees-of-freedom enter the global system of equations. Effectively, a penalty-type approach then results.

While studies in which the performance of such elements for rubber-like material behaviour have been reported for two-dimensional finite elements (plane–strain conditions)[17], the literature does not seem to be overflowing of investigations of the behaviour of three-dimensional finite elements for rubber-like behaviour, albeit some interesting studies have been reported for fluid flow[5]. Here, the additional complication arises that a formal assessment by the LBB condition[11], which can be used to rigorously determine the ability of finite elements to deform properly under isochoric conditions, is quite difficult already for two-dimensional elements, let alone for three-dimensional elements. In this contribution a more heuristic approach is therefore followed. First, the ability of some three-dimensional finite elements with separate interpolations for the pressures and the displacements is estimated using the constraint-counting method[6,10]. Then, the performance of the elements is further assessed in numerical simulations of bearing blocks for different ratios of the height over the width of the block. These numerical simulations suggest that the balance of the number of degrees-of-freedom for the displacements vs. the pressure degrees-of-freedom is quite delicate, since too many pressure degrees-of-freedom makes the element overstiff, but too few pressure degrees-of-freedom tend to cause a premature break-down of the calculations because of the occurrence of spurious kinematic modes, a phenomenon that has also been observed in non-linear calculations of concrete cracking[4].

RUBBER-LIKE MATERIAL BEHAVIOUR

It is assumed that rubber can be characterized as an isotropic, non-linear elastic material. In this approach the mechanical behaviour is assumed to be time and temperature-independent and is described fully by a strain–energy function:

$$W = W(I_1, I_2, I_3) \tag{1a}$$

with I_i the invariants of the right Cauchy–Green stretch tensor $\mathbf{C}$. The Mooney–Rivlin model is an example of a strain–energy function which is formulated in this manner. Especially for compressive-shear loadings the Mooney–Rivlin approach does not capture the mechanical behaviour of rubbers very accurately[2], and approaches that set out to describe the mechanical behaviour of rubbers via principal stretches are more successful. Then,

$$W = W(\lambda_1, \lambda_2, \lambda_3) \tag{1b}$$

with λ_i the principal stretches of $\mathbf{C}$. The models proposed by Ogden[12] and Peng and Landel[14] fall within this class. For the purpose of this study, i.e. the assessment of the behaviour of

three-dimensional finite elements in nearly incompressible finite elasticity, the precise form of the strain–energy function is not so important. Since invariant-based models are somewhat easier to implement, such a model, namely the above-mentioned Mooney–Rivlin model,

$$W = K_1(I_1 - 3) + K_2(I_2 - 3) \tag{2}$$

with K_1 and K_2 material parameters, has been used in the example calculations. To emphasize the irrelevance of the choice of either invariants or principal stretches to formulate the strain–energy function for our purpose, we will write (1) in the compact manner:

$$W = W(\chi) \tag{3}$$

where χ contains the basic parameters that define the state of deformation in a material point.

Classically, rubbers have been assumed to be strictly incompressible, i.e. the following constraint is imposed in terms of the relative volume change,

$$J = \frac{V}{V_0} = \sqrt{\det(\mathbf{C})} = 1 \tag{4a}$$

or in terms of principal stretches,

$$\lambda_1 \lambda_2 \lambda_3 = 1 \tag{4b}$$

so that W purely describes deviatoric deformations. The quantity J is defined as the quotient of the actual volume V of a body and its corresponding volume in the reference configuration V_0.

The assumption of a strictly incompressible material can be relaxed by introducing additional terms in the strain–energy function W. Such a strain–energy function has first been introduced by Penn[16] and is formulated by a modified set of basic parameters $\tilde{\chi}$, which is used to formulate the distortional part of the strain–energy function W_d, and by the relative volume change J, which is employed for the definition of the hydrostatic part of the strain–energy function W_h:

$$W = W_d(\tilde{\chi}) + W_h(J) \tag{5}$$

Typically, W_d is of the order μ and W_h is of the order κ, μ and κ being the ground-state shear modulus and the bulk modulus, respectively. Although it has been demonstrated[13,15,16] that even this approach does not predict the volume change with sufficient accuracy, especially in combined shear–compressive loadings[2], additional terms are not introduced in (5), since this issue is of no importance for the aim of the present study.

The second Piola–Kirchhoff stress σ can be calculated by differentiation of W with respect to the right Cauchy–Green stretch tensor:

$$\sigma = 2\frac{\partial W}{\partial \mathbf{C}} \tag{6}$$

or, using the decomposition of the strain–energy function into a deviatoric part W_d and a hydrostatic part W_h:

$$\sigma = \sigma_d + \sigma_h \tag{7}$$

with

$$\sigma_d = 2\frac{\partial W_d}{\partial \mathbf{C}} \tag{8a}$$

and

$$\boldsymbol{\sigma}_h = 2p\frac{\partial J}{\partial \mathbf{C}} \tag{8b}$$

p being the hydrostatic pressure.

As for the deviatoric part of the strain–energy function several formulations also exist for the hydrostatic part. Generally,

$$p = \kappa f_p(J) \tag{9a}$$

where the bulk modulus κ is supposed to be a constant within the considered range of volume changes. In the present study, a linear relationship has been adopted for f_p,

$$f_p = J - 1 \tag{9b}$$

which is valid for pressures up to hundreds of atmospheres[18]. Note that p is negative in compression for this definition.

The incremental stress–strain relation is obtained by differentiating (6)–(8) once more, yielding

$$\Delta\boldsymbol{\sigma} = \mathbf{D}\Delta\gamma + \Delta p\mathbf{d} \tag{10}$$

with $\gamma = \frac{1}{2}(\mathbf{C} - \mathbf{I})$ the Green–Lagrange strain tensor,

$$\mathbf{D} = 4\frac{\partial^2 W}{\partial \mathbf{C}^2} + 4p\frac{\partial^2 J}{\partial \mathbf{C}^2} \tag{11a}$$

and

$$\mathbf{d} = 2\frac{\partial J}{\partial \mathbf{C}} \tag{11b}$$

FINITE ELEMENT FORMULATION

When the ratio of bulk modulus over ground-state shear modulus κ/μ tends to infinity, unbounded stiffness terms are created. To avoid locking phenomena a finite element formulation is then necessary in which the displacements $\mathbf{u}$ as well as the hydrostatic pressure p are treated as a fundamental unknown in the boundary-value problem. As a point of departure for the derivation of the governing finite element equations, the virtual work expression[1,3,6]:

$$\int_{V_0} \delta\boldsymbol{\gamma}^{\mathrm{T}}\boldsymbol{\sigma}^{t+\Delta t}\,\mathrm{d}V_0 = \int_{V_0} \rho_0 \delta\mathbf{u}^{\mathrm{T}}\mathbf{g}\,\mathrm{d}V_0 + \int_{S_0} \delta\mathbf{u}^{\mathrm{T}}\mathbf{t}_0\,\mathrm{d}S_0 \tag{12}$$

and the weak form of the hydrostatic pressure–volume change relation (9):

$$\int_{V_0} [f_p^{t+\Delta t} - \kappa^{-1}p^{t+\Delta t}]\delta p\,\mathrm{d}V_0 = 0 \tag{13}$$

are taken. In (12) and (13), the subscript 0 refers to the undeformed configuration or ground state, while the superscript $t+\Delta t$ indicates that the value of a quantity is considered at 'time' $t+\Delta t$. The superscript T denotes a transpose, the δ-symbol denotes the first variation of a quantity, ρ is the mass density and $\mathbf{g}$ the gravity acceleration vector, $\mathbf{t}$ represents the normal tractions on the surface of the body and $\mathbf{u}$ is the displacement vector. The strain $\gamma = \varepsilon + \eta$ consists of a part ε that is linear in the displacements $\mathbf{u}$ and part η that is quadratic in $\mathbf{u}$. Decomposing the stress $\sigma^{t+\Delta t}$ in an additive fashion as the sum of the stress σ^t at 'time' t, the beginning of

the loading step, and a stress increment $\Delta\sigma$, substituting the incremental stress–strain relation (10) and linearizing in the sense that second-order terms in the incremental displacements $\Delta\mathbf{u}$ are neglected, (12) can be recast as[3]:

$$\int_{V_0} \delta\boldsymbol{\varepsilon}^{\mathrm{T}}\mathbf{D}\Delta\boldsymbol{\varepsilon}\,\mathrm{d}V_0 + \int_{V_0} \delta\boldsymbol{\eta}^{\mathrm{T}}\boldsymbol{\sigma}^t\,\mathrm{d}V_0 + \int_{V_0} \delta\boldsymbol{\varepsilon}^{\mathrm{T}}\mathbf{d}\Delta p\,\mathrm{d}V_0 = \int_{V_0} \rho_0\delta\mathbf{u}^{\mathrm{T}}\mathbf{g}\,\mathrm{d}V_0 + \int_{S_0} \delta\mathbf{u}^{\mathrm{T}}\mathbf{t}_0\,\mathrm{d}S_0 - \int_{V_0} \delta\boldsymbol{\varepsilon}^{\mathrm{T}}\boldsymbol{\sigma}^t\,\mathrm{d}V_0 \tag{14}$$

By a similar decomposition with respect to the pressure, $p^{t+\Delta t} = p^t + \Delta p$, and invoking identity (11b) we can rewrite (13) as:

$$\int_{V_0} \delta p\mathbf{d}^{\mathrm{T}}\Delta\boldsymbol{\gamma}\,\mathrm{d}V_0 - \kappa^{-1}\int_{V_0} (f_p')^{-1}\Delta p\delta p\,\mathrm{d}V_0 = -\int_{V_0} (f_p')^{-1}[f_p' - \kappa^{-1}p^t]\delta p\,\mathrm{d}V_0 \tag{15}$$

where the prime denotes differentiation with respect to J. For the simple choice (9b) obviously $f_p' = 1$.

For the spatial discretization it is assumed that the contiuum is divided in an arbitrary number of finite elements and that the part of the strain increment $\Delta\boldsymbol{\varepsilon}$ that is linear in the incremental displacements $\Delta\mathbf{u}$ can be written as:

$$\Delta\boldsymbol{\varepsilon} = \mathbf{L}\Delta\mathbf{u} = \mathbf{L}\mathbf{H}\Delta\mathbf{a} = \mathbf{B}_L\Delta\mathbf{a} \tag{16}$$

with $\Delta\mathbf{a}$ the incremental nodal displacement vector and $\mathbf{H}$ the matrix collecting the interpolation polynomials for the displacements. $\mathbf{L}$ contains differential operators which represent the kinematic relation between the displacements and the linear part of the strain tensor γ. Since p has been assumed to be an independent variable a separate interpolation is necessary for the pressure. Because of its origin as an additional constraint no explicit boundary conditions are required for the pressure field and a wider range of interpolations is permissible than for the displacement field. Furthermore, the pressure degrees-of-freedom can be introduced either as system or element degrees-of-freedom[1,6,7]. The latter approach, which has been followed in this study, implies a discontinuous pressure field across the element boundaries. Assembling the interpolation polynomials for the pressure degrees-of-freedom in the matrix $\mathbf{N}$, we have:

$$\Delta p = \mathbf{N}\Delta\mathbf{p} \tag{17}$$

where $\Delta\mathbf{p}$ contains the values of the incremental pressures in the nodes.

Substitution of the relations (16) and (17) in (14) and (15) the relation between the incremental displacements and pressure and the external forces becomes

$$\begin{bmatrix} \mathbf{K}_a & \mathbf{K}_p \\ \mathbf{K}_p^{\mathrm{T}} & \kappa^{-1}\mathbf{M} \end{bmatrix}\begin{bmatrix} \Delta\mathbf{a} \\ \Delta\mathbf{p} \end{bmatrix} = \begin{bmatrix} \mathbf{F}_a \\ \mathbf{F}_p \end{bmatrix} \tag{18}$$

In (18) the following definitions have been utilized:

$$\mathbf{K}_a = \int_{V_0} \mathbf{B}_L^{\mathrm{T}}\mathbf{D}\mathbf{B}_L\,\mathrm{d}V_0 + \int_{V_0} \mathbf{B}_{NL}^{\mathrm{T}}\Sigma\mathbf{B}_{NL}\,\mathrm{d}V_0 \tag{19}$$

$$\mathbf{K}_p = \int_{V_0} \mathbf{B}_L^{\mathrm{T}}\mathbf{d}\mathbf{N}\,\mathrm{d}V_0 \tag{20}$$

$$\mathbf{M}_p = -\int_{V_0} (f_p')^{-1}\mathbf{N}^{\mathrm{T}}\mathbf{N}\,\mathrm{d}V_0 \tag{21}$$

$$\mathbf{F}_a = \int_{V_0} \rho_0 \mathbf{H}^{\mathrm{T}} \mathbf{g}\, \mathrm{d}V_0 + \int_{S_0} \mathbf{H}^{\mathrm{T}} \mathbf{t}_0\, \mathrm{d}S_0 - \int_{V_0} \mathbf{B}_L^{\mathrm{T}} \boldsymbol{\sigma}'\, \mathrm{d}V_0 \tag{22}$$

$$\mathbf{F}_p = \int_{V_0} (f_p')^{-1} \mathbf{N}^{\mathrm{T}} [f_p^t - \kappa^{-1} p']\, \mathrm{d}V_0 \tag{23}$$

where the additional symbols $\boldsymbol{\Sigma}$ and $\mathbf{B}_{NL}$ have been introduced for the matrix representation of the 2nd Piola–Kirchhoff stress tensor and the relation between the non-linear part of the strain tensor and the displacements, respectively[1].

CONSTRAINT COUNTING

For the calculation of the element stiffness matrix in (18) independent interpolation polynomials can be chosen for the displacement and pressure field. An arbitrary combination of interpolation functions, however, may lead to a poor numerical performance. Therefore, it is desirable to determine the ratio between the number of displacement degrees-of-freedom and pressure degrees-of-freedom which ensures an optimal numerical performance. For mixed finite elements a sound mathematical theory is available through the Ladyzenskaya–Babuska–Brezzi (LBB) condition[11]. Unfortunately, proofs that an element passes the LBB condition are notoriously difficult. The method is therefore not a handy tool to judge the performance of finite elements. Instead, a simple and heuristic method, based on the constraint-counting method[6,10], will be applied to mixed elements with a discontinuous pressure field. This prediction will be followed by an assessment of the performance of the various alternatives that seem reasonable on the basis of the above-mentioned quick-look procedure.

To provide a proper setting, the fundamental difficulty in (nearly) incompressible elasticity is recalled by means of *Figure 1*, in which a four-noded quadrilateral two-dimensional element is plotted with eight displacement degrees-of-freedom. At the left and bottom edges prescribed zero displacements have been imposed, so that the model possesses just two degrees-of-freedom. We may now envisage a model composed of an arbitrary number of these basic elements. Each element that is added in either direction increases the total number of displacement

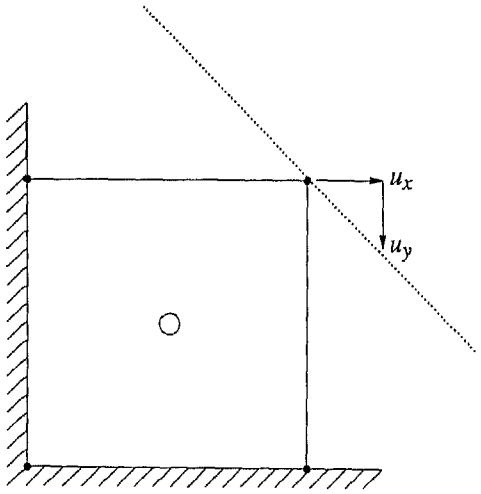

Figure 1 Restricted movement of 'free' node in an incompressible medium

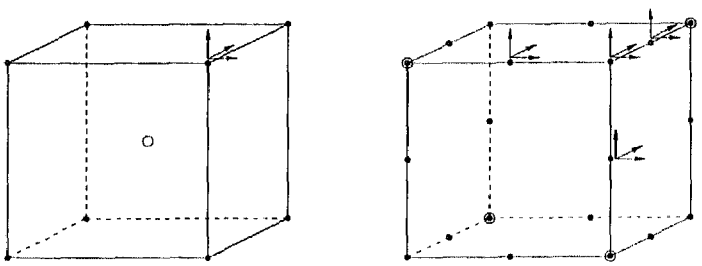

• Displacement nodes o Pressure nodes

Figure 2 Displacement nodes and pressure nodes for 8/1 and 20/4 elements

degrees-of-freedom by two. The assumption of incompressibility implies a constant surface of the element, and, as a consequence, a restricted movement of the free node along the dashed line. The restricted freedom of the node is established by an additional constraint equation by means of *one* pressure degree-of-freedom. When two or more pressure points are specified no displacement degrees-of-freedom are left, which phenomenon is referred to as mesh locking. When, on the other hand, no pressure points are introduced spurious kinematic modes may arise during the numerical simulation. In sum, it can be concluded that for two-dimensional elements the optimal ratio $r = n_d/n_p$ of the number of displacement degrees-of-freedom n_d over the number of pressure points n_p equals two, while for three-dimensional elements the optimal ratio $r = 3$. The problems of mesh locking and spurious kinematic modes are only marginally ameliorated for *nearly* incompressible material behaviour and, therefore, a mixed finite element formulation consisting of displacement degrees-of-freedom and pressure degrees-of-freedom is also needed in this case.

The utilized method suggests an influence of the boundary conditions on the number of constraint conditions. In fact, the ratio r of the whole finite element model should be considered to determine the optimal number of pressure degrees-of-freedom. Also, the number of constraint conditions should be distributed inhomogeneously over the element mesh in order to arrive at a locally optimal ratio: fewer pressure degrees-of-freedom near edges with a prescribed displacement and more pressure degrees-of-freedom near edges with a prescribed boundary traction. This proposition will be taken up again in a later section. It is emphasized that the idea is not rooted in a firm mathematical theory, but is a practical approach to obtain an estimate of the robustness of finite elements in nearly incompressible rubber elasticity.

The method outlined above has been applied to determine the optimal number of pressure points in three-dimensional elements. In *Figure 2* two isoparametric serendipity hexahedrons are plotted with a trilinear and a triquadratic displacement field, respectively. The trilinear element is referred to as the 8/1 element, because of its eight displacement nodes and one pressure node. Similarly, the triquadratic element with four pressure degrees-of-freedom is denoted by 20/4, while the triquadratic element with one pressure node is labelled as 20/1. The latter element has primarily been included in the discussion to gain some insight in the influence of the number of pressure points on the numerical performance of twenty-noded elements. Since the ratio r of the 20/1 element is significantly higher than three we may expect a rather unstable displacement field at higher deformation levels.

INTERPOLATION SCHEME 20/4 ELEMENT

The 8/1 and 20/1 element possess a trivial constant interpolation polynomial for the pressure field. The 20/4 element needs a linear four-point interpolation polynomial in a three-dimensional

space, which can be derived by degeneration of the trilinear shape functions, which are also used to describe the displacement degrees-of-freedom of the 8/1 element. Now, let $\boldsymbol{\xi}=(\xi,\eta,\zeta)$ be the isoparametric place vector and $\mathbf{x}=(x,y,z)$ be the place vector in model coordinates. Then, the mapping of a point from model to isoparametric coordinates is defined by the shape functions N_i according to:

$$\mathbf{x}(\boldsymbol{\xi})=\sum_{i=1}^{n} N_i(\boldsymbol{\xi})\mathbf{x}_i^e \tag{24}$$

where $\mathbf{x}_i^e$ are the model coordinates of node i and element e and n is the number of element nodes.

The degeneration process implies the mapping of more than one point in the $\boldsymbol{\xi}$-space on a point in the $\mathbf{x}$-space. A proper linear shape function is obtained when four independent points span a three-dimensional space. To meet this requirement and to obtain a symmetric set of polynomials the following degeneration has been employed:

$$\begin{aligned} N_1^*&=N_1+N_2=\tfrac{1}{4}(1-\eta)(1-\zeta)\\ N_3^*&=N_3+N_4=\tfrac{1}{4}(1+\eta)(1-\zeta)\\ N_6^*&=N_6+N_7=\tfrac{1}{4}(1+\xi)(1+\zeta)\\ N_8^*&=N_8+N_5=\tfrac{1}{4}(1-\xi)(1+\zeta) \end{aligned} \tag{25}$$

It is noted that this interpolation scheme satisfies the basic convergence requirements with respect to the smoothness on the element domain V^e and completeness[1,6], but that continuity across the element boundaries S^e is lost due to the degeneration process. Because of the assumed element-wise condensation of the pressure degrees-of-freedom this is of no further consequence here.

PERFORMANCE

The performance of the three mixed elements will be demonstrated by numerical simulations on three cuboidal rubber blocks loaded in compression. Each rubber block has a different shape factor which is defined as[8]:

$$f_s=\frac{\text{loaded surface}}{\text{unloaded surface}}=\frac{BL}{H(B+L)} \tag{26}$$

with B the width, H the height and L the length of the block. The blocks are compressed by prescribing uniform displacements on the top face, while the sides are free to bulge out. Additional calculations in which the performance of the elements is studied by imposing a rotation to the top face have also been carried out. Block II, which is shown in *Figure 3*, will henceforth be taken as the reference block[3]. The other two blocks have a higher shape factor (Block I) and a lower shape factor (Block III) respectively. As can be observed from the definition in (26) a higher shape factor means a more stubby specimen, while a lower shape factor implies a more slender specimen. The finite element discretization for the linear 8/1 element has been chosen such that the total number of displacement degrees-of-freedom is approximately equal to that of the mesh for the quadratic elements. All calculations have been carried out with the following (representative) material parameters: $K_1=0.49\ \text{N/mm}^2$, $K_2=0.16\ \text{N/mm}^2$ and $\kappa=1000\ \text{N/mm}^2$. Since the ground-state shear modulus μ is now equal to $1.3\ \text{N/mm}^2$, these data result in a κ/μ ratio of approximately 770.

Block II, the reference block, has the dimensions $200\times 100\times 33\ \text{mm}^3$, which results in a shape

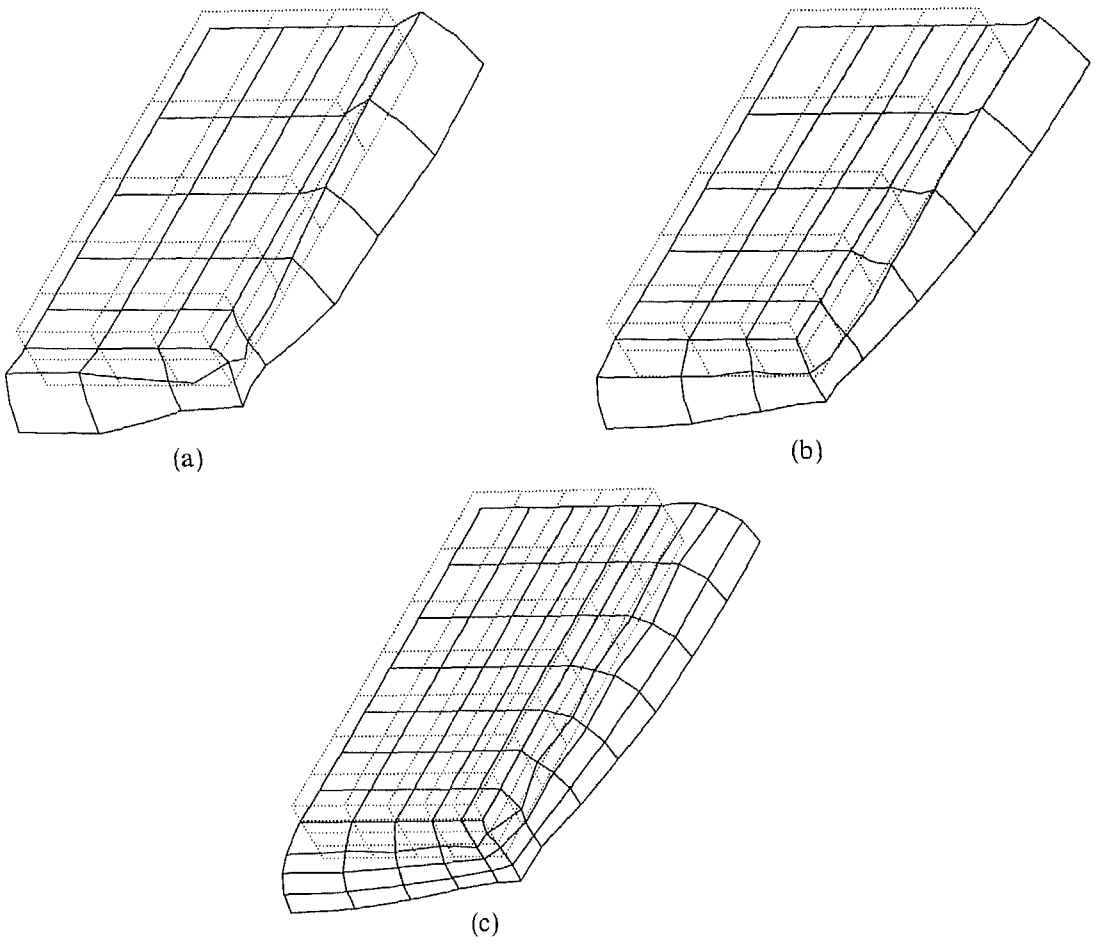

Figure 3 Undeformed and deformed finite element models for block II after 30% compression. (a) 20/1 element; (b) 20/4 element; (c) 8/1 element

factor $f_s = 2.02$ according to definition (26). Because of symmetry considerations only one-eighth of the layer had to be modelled. This has been done with 30 quadratic elements (*Figures 3a* and *3b*) and with 140 linear elements (*Figure 3c*) respectively. *Figure 3* shows the deformed models at 30% compression, i.e., at a level where the deformed block has 70% of its original height. For the 20/1 element (*Figure 3a*) we observe a slightly irregular displacement field along the long side of the block, which is not observed for the mesh with 20/4 element (*Figure 3b*). The 8/1 element, on the other hand, gives rise to severe local spurious mechanisms.

A notable observation is also that spurious kinematic modes are already observed after 16% compression for the 20/1 element, but that a smooth displacement field is retrieved at a higher load level. This phenomenon, which is quite characteristic, has also been visualized in *Figure 4*, in which the relation between the *horizontal* displacement of the midside node of the long side and the compression level has been plotted. Up to 16% compression bulging of the side grows linearly with the compression level, but decreases between approximately 18% and 22%, while the curves obtained from the calculations for the meshes with the 8/1 and 20/4 elements are monotonically increasing. *Figure 5*, in which the vertical force–vertical displacement relation

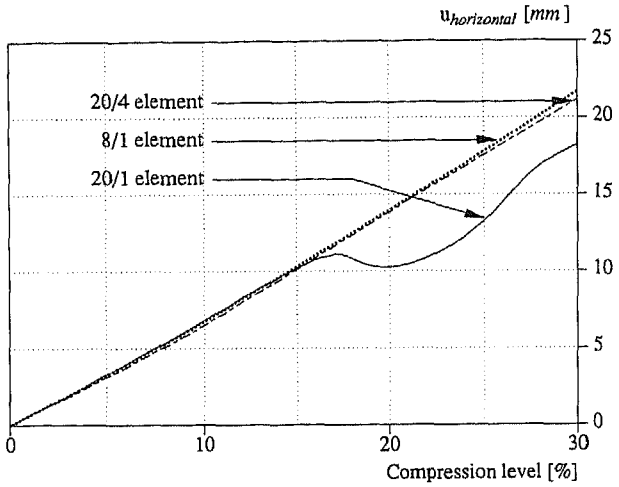

Figure 4 Horizontal displacement of different nodes along the long side as a function of the vertical compression

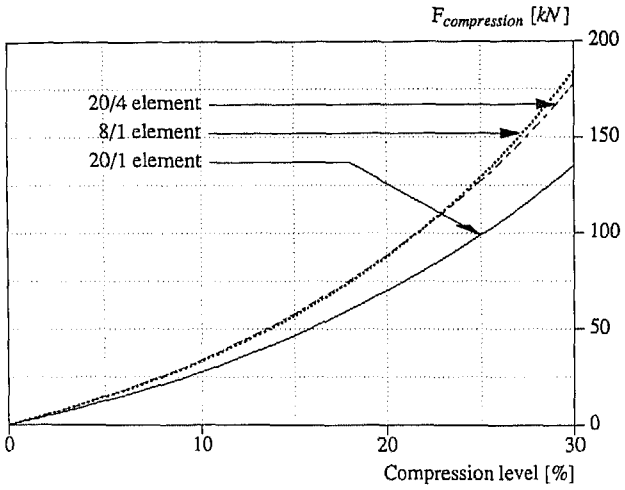

Figure 5 Compressive force vs. vertical displacement of the top face

has been plotted for the three elements types, clearly shows the stiffening influence of an increase of the number of pressure nodes, since the 8/1 and 20/4 elements react definitely stiffer than the 20/1 element.

For the geometry of block II the behaviour of the elements has also been studied in case of a rotation of the top face. For this loading condition the prescribed displacements are kept zero on one of the short sides and are pushed downwards on the opposing side, while the prescribed displacements between the two sides were prescribed according to a linear interpolation. *Figure 6* shows one-quarter of a rubber layer and its state of deformation at 30% compression (at one side). The 20/1 element obviously possesses too few pressure nodes to avoid spurious kinematic modes, while the 20/4 element is largely free from this phenomenon. Yet, near the corner of the block also the displacement fields that were computed using the 8/1 and 20/4 elements show

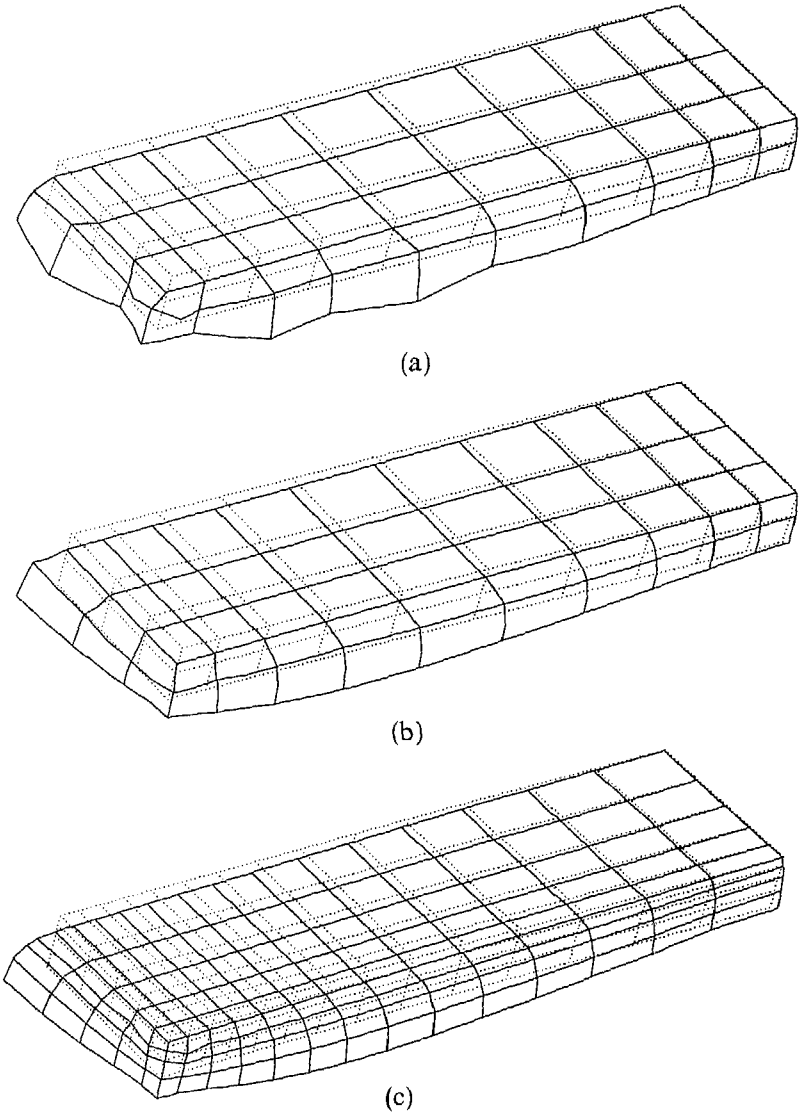

Figure 6 Undeformed and deformed finite element models for block II after 30% compression of one of the short sides. (a) 20/1 element; (b) 20/4 element; (c) 8/1 element

some mild forms of spurious mechanisms. This observation confirms the prediction of the constraint-counting approach, namely that the 20/1 element would satisfy the incompressibility constraint, but would easily give rise to the occurrence of spurious mechanisms, whereas the 8/1 and 20/4 elements would behave better. Nevertheless, near the corners of the meshes the number of pressure points is not sufficient also for the 8/1 and 20/4 elements.

The second block, labelled as I, has the dimensions $940 \times 940 \times 99\,\text{mm}^3$ and a shape factor $f_s = 4.75$. The finite element models, shown in *Figure 7*, consist of 98 twenty-noded elements and 363 eight-noded elements respectively. From the deformed element meshes it can be seen that even the model with the 20/1 elements is (almost) free from spurious kinematic modes.

Finally, a block with a height of 150 mm, a length of 200 mm and a width of 150 mm has

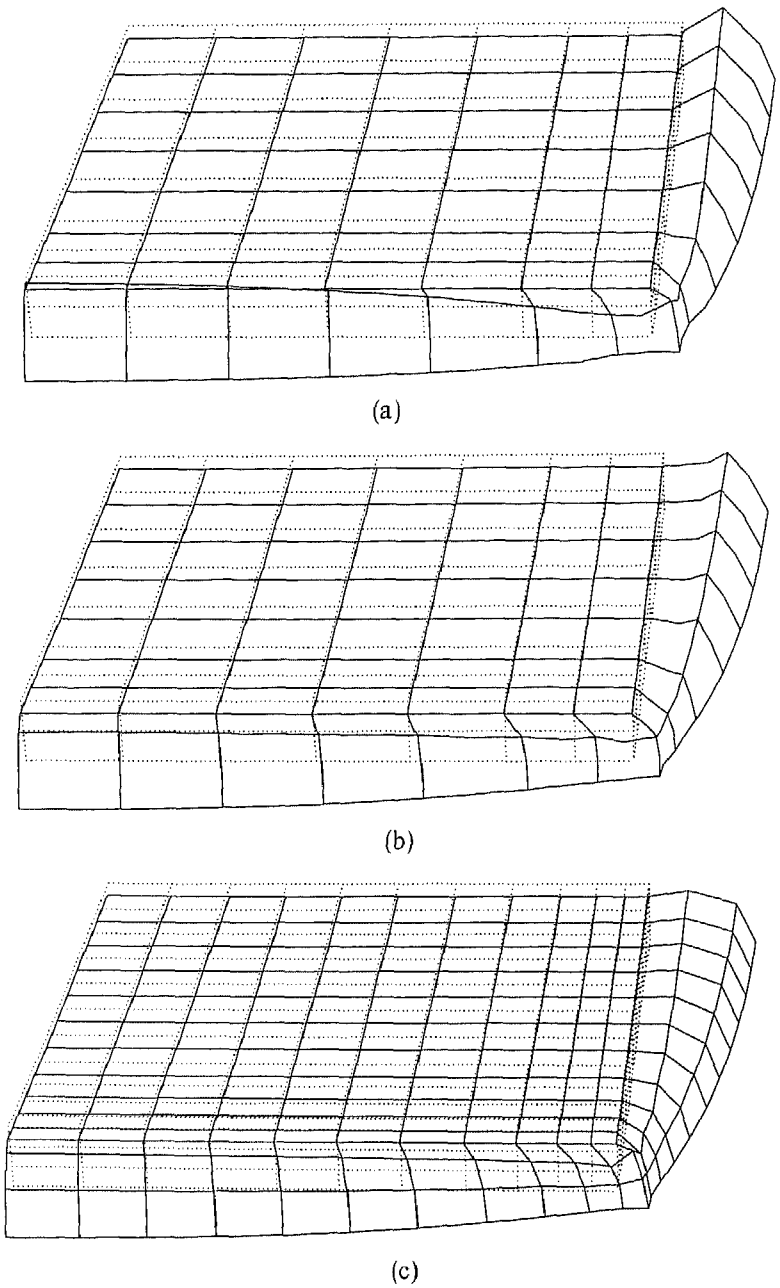

Figure 7 Undeformed and deformed finite element models for block I loaded in pure compression. (a) 20/1 element; (b) 20/4 element; (c) 8/1 element

been studied (block III). The shape factor of this rather slender block is $f_s = 0.51$. From *Figure 8* it can be seen that a block with this shape factor is rather sensitive to spurious mechanisms. For each type of element the results show irregularities in the displacement field, although the extent varies with the type of element.

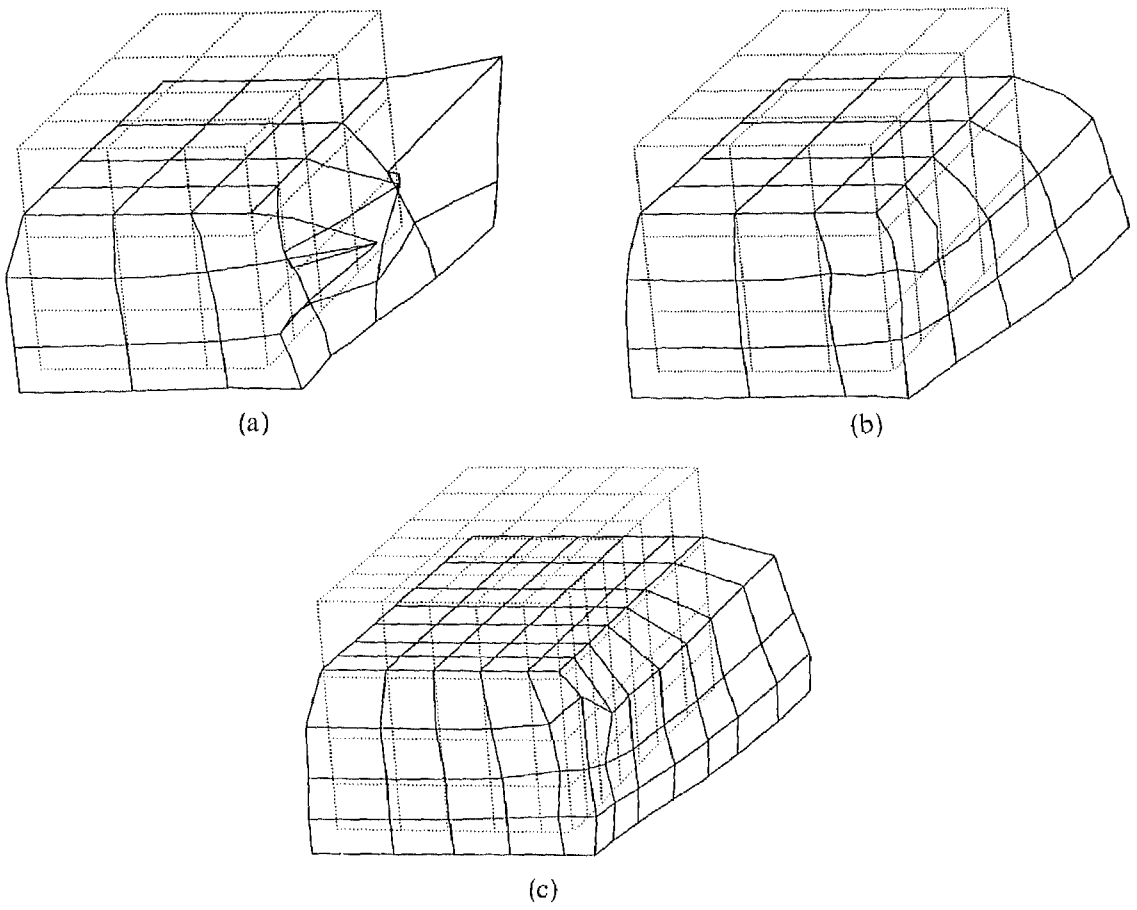

Figure 8 Undeformed and deformed finite element models for block III loaded in pure compression. (a) 20/1 element; (b) 20/4 element; (c) 8/1 element

DISCUSSION

In *Table 1* the main aspects of this study have been summarized. For each geometry a row is included giving the ratio r of the number of displacement degrees-of-freedom over the number of pressure degrees-of-freedom. In the rows 'spurious modes' the percentage (in terms of the vertical displacement over the height of the specimen) is given at which smoothness of the displacement field along the sides is lost. The rows called 'convergence' refer to the displacement level at which no converged solution could be found using a modified Newton–Raphson iterative procedure for a step size of 1% compression. This criterion implies that convergence could still be achieved for smaller step sizes, or when using a full Newton–Raphson procedure.

From *Table 1* is can be concluded that, when the optimal ratio $r=3.0$ is satisfied for a three-dimensional finite element mesh, the point where the analysis has to be abandoned is not governed by spurious mechanisms. Then, convergence problems arise at approximately the same load level. Indeed, the tendency can be observed that the convergence behaviour becomes more critical at higher shape factors compared with the occurrence of spurious mechanisms. Put differently, the point where an analysis has to be terminated is governed by failure of the iterative process for stubby specimens (a high shape factor), while for more slender specimens (a lower

Table 1 Performance of the elements

Element type	20/1	20/4	8/1
Block I ($f_s=4.75$)			
$r=n_a/n_p$	12.0	3.00	2.97
spurious modes	20%	25%	25%
convergence	18%	23%	25%
Block II ($f_s=2.02$)			
$r=n_a/n_p$	11.3	2.83	3.40
spurious modes	16%	>48%	30%
convergence	18%	43%	32%
Block III ($f_s=0.51$)			
$r=n_a/n_p$	14.4	3.60	3.40
spurious modes	20%	30%	50%
convergence	30%	52%	53%

shape factor) the emergence of spurious mechanisms marks the point where meaningful solutions can no longer be obtained. Some subtle differences exist between the different types of elements, since the 8/1 and especially the 20/1 element are more sensitive to spurious mechanisms than the 20/4 element.

Although *Table 1* clearly reveals some tendencies a direct relation between the sensitivity to spurious kinematic modes and the shape factor cannot be extracted on the basis of the available information. The simulations with the 8/1 element (block I) show local irregularities, although the element has the same ratio r as the 20/4 element. When more elements are used over the height of the specimen the problem becomes even worse[9], since a larger number of displacement degrees-of-freedom is added to the system of equations than constraint equations. This observation suggests that the number of pressure nodes should be increased with a diminishing number of prescribed displacements, so that the ratio r remains optimal.

Near the corners of the specimens the number of displacement degrees-of-freedom is relatively larger than the number of pressure degrees-of-freedom. Apparently, this can lead to local irregularities. Just as the global ratio r indicates the sensitivity to global spurious kinematic modes, the 'local' value of r seems to determine whether local spurious mechanisms can arise. It is therefore suggested that the number of pressure degrees-of-freedom in the elements near these corners should be raised. For this purpose only elements with a discontinuous pressure field can be used.

CONCLUSIONS

The heuristic method of constraint counting for determining the capabilities of mixed elements under (nearly) isochoric deformations gives a reasonable prediction for applications in finite elasticity. When supplemented by extensive numerical testing a good assessment can be made of the element behaviour. The optimal ratio r between displacement degrees-of-freedom and pressure degrees-of-freedom should locally and globally be satisfied to suppress spurious kinematic modes. Since this ratio also is affected by the boundary conditions of the finite element model a variable number of pressure degrees-of-freedom is suggested. This can only be achieved by using elements with a discontinuous pressure field across the element boundaries. The use of an element mesh with a homogeneous distribution of incompressibility constraints and a global optimal ratio may still lead to the occurrence of local spurious mechanisms.

It has been found that the shape factor of a cuboidal block influences the load level until which a converged solution can be obtained. Apparently, an optimal ratio between displacement degrees-of-freedom and pressure degrees-of-freedom assures that neither the convergence of the iterative procedure, nor the occurrence of spurious mechanisms cause a premature termination of the analysis.

ACKNOWLEDGEMENTS

The example calculations have been carried out with the finite element package DIANA of the TNO Institute of Building Materials and Structures.

REFERENCES

1 Bathe, K.-J. *Finite Element Procedures in Engineering Analysis*, Prentice-Hall, Englewood Cliffs, NJ (1982)
2 van den Bogert, P. A. J. and de Borst, R. Constitutive aspects and finite element analysis of 3D rubber specimens in compression and shear, in *Proc. Third Int. Conf. Numerical Methods in Engineering: Theory and Applications (NUMETA90)* (Eds G. N. Pande and J. Middleton), Elsevier Applied Science, London-New York, pp. 870–877 (1990)
3 de Borst, R., van den Bogert, P. A. J. and Zeilmaker, J. Modelling and analysis of rubberlike materials, *HERON*, **33** (1), 1–57 (1988)
4 de Borst, R. and Rots, J. G. Occurrence of spurious mechanisms in computations of strain-softening solids, *Eng. Comput.* **6**, 272–280 (1989)
5 Engelman, M. S., Sani, R. L., Gresho, P. M. and Bercovier, M. Consistent vs. reduced integration penalty methods for incompressible media using several old and new elements, *Int. J. Num. Meth. Fluids*, **2**, 25–52 (1982)
6 Hughes, T. J. R. *The Finite Element Method. Linear Static and Dynamic Analysis*, Prentice-Hall, Englewood Cliffs, NJ (1987)
7 Jankovich, E., Leblanc, F., Durand, M. and Bercovier, M. A finite element method for the analysis of rubber parts, experimental and analytical assessment, *Comput. Struct.*, **14**, 385–391 (1981)
8 Lindley, P. B. *Engineering Design with Natural Rubber*, 3rd Edn, Malaysian Rubber Producers' Research Association, Welwyn (1970)
9 Luiten, G. T. Optimisation of a 3-D element for rubberlike materials (in Dutch), *TNO-IBBC Report BI-89-096/72.8.8003*, Delft (1989)
10 Nagtegaal, J. C., Parks, D. M. and Rice, J. R. On numerically accurate finite element solutions in the fully plastic range, *Comp. Meth. Appl. Mech. Eng.*, **4**, 153–177 (1974)
11 Oden, J. T. and Carey, G. F. *Finite Elements: Mathematical Aspects*, Vol. IV., Prentice-Hall, Englewood Cliffs, NJ (1984)
12 Ogden, R. W. Large deformation isotropic elasticity: on the correlation of theory and experiment for incompressible rubberlike solids, *Proc. R. Soc.*, **A326**, 565–584 (1972)
13 Ogden, R. W. Volume changes associated with the deformation of rubberlike solids, *J. Mech. Phys. Solids*, **24**, 323–338 (1976)
14 Peng, S. T. J. and Landel, R. F. Stored energy function of rubberlike materials derived from simple tensile data, *J. Appl. Phys.* **43**, 3063–3067 (1972)
15 Peng, S. T. J. and Landel, R. F. Stored energy function and compressibility of compressible rubberlike materials under large strain, *J. Appl. Phys.* **46**, 2599–2604 (1975)
16 Penn, R. W. Volume changes accompanying the extension of rubber. *Trans. Soc. Rheol.*, **14**, 509–517 (1970)
17 Sussman, T. and Bathe, K.-J. A finite element formulation for nonlinear incompressible elastic and inelastic analysis, *Comput. Struct.*, **26**, 357–409 (1987)
18 Wood, L. A. and Martin, G. M. Compressibility of natural rubber at pressures below 500 kg/cm^2, *NBS J. Res.*, **68A**, 259–268 (1964)